Infrared and Liquid Chromatographic Characterization of Epoxy Cresol Novolac-Phenol Formaldehyde Novolac-Tertiary Amine Resin Systems

D. J. BELTON and E. SULLIVAN, *Philips Research Laboratories, Sunnyvale, Signetics Corp., P.O. Box 3408, 811 E. Arques Ave., Sunnyvale, California, 94088-3409.*

Synopsis

The subject of this paper is an infrared and liquid chromatographic characterization of epoxy molding compounds of importance in the microelectronic manufacturing industry. A complete infrared description of resin extracts from 4000 to 700 cm^{-1} is given for three nondisclosed commercial extracts via comparisons with model epoxy cresol novolac and phenol formaldehyde novolac resins and by observing those spectral alterations affected during cure. In addition, both the molecular weight distributions and the methodology of obtaining such for the resin and hardener components of the extracts are described. These results are based upon reversed phase liquid chromatography and infrared spectroscopic measurements. The analysis described in this paper demonstrates significant differences among materials that, by chromatography alone, appear to have only subtle variations in both the resin and hardener molecular weight distributions. These differences include not only the quantity of resin or hardener of a particular oligomeric molecular weight, but also the apparent resin-to-hardener stoichiometry of the combined system.

INTRODUCTION

Thermosetting epoxy resin systems are becoming increasingly important in the packaging of integrated circuits. Consider, for example, the rapid evolution of formulations and the inclusion of fast-cure, low-stress, and low-α-particle systems in the range of products offered. Molding compounds used in electronic applications are typically based upon a silica-filled epoxy cresol novolac (ECN)-phenol formaldehyde novolac (PFN)-tertiary amine system. These systems are modified based upon the needs of the user to include such additives as mold release agents, flame retardants, diluents, and dyes. The complexity, rapid evolution of formulations, and failures associated with field service place an increasing amount of importance upon understanding basic structure-property relationships in these systems by the end user.

Such properties of a thermosetting epoxy resin system as resin-hardener stoichiometry, resin and hardener molecular weight distributions, catalyst chemistry, and catalyst concentration are known to affect both the curing kinetics and the microstructure of the final product.[1-10] There is, however, a paucity of information available on studies of the aforementioned nature and chemical characterizations in the ECN-PFN-tertiary amine system. It

Journal of Applied Polymer Science, Vol. 31, 1309–1326 (1986)
 CCC 0021-8995/86/051309-18$04.00

is therefore, the intent of this paper to address the subject of the physical and chemical characterization of molding compound resin systems which is the first step in a study aimed at establishing structure-property relationships in this commercially important system.

Experimental

Standards of an epoxy cresol novolac and a phenol formaldehyde novolac were supplied by Ciba-Geigy (ECN1273), and Schenectady Chemicals (HRJ1166), respectively. Commercially available molding compound resins will be designated as resin system A, resin system B, and resin system C rather than by their manufacturer's product number. The resins were extracted from the B-staged pellets using tetrahydrofuran (THF) and filtered through a 0.2-μm acetate filter.

Infrared spectra were measured on a Digilab FTS-20C Fourier transform infrared spectrophotometer (IRS) equipped with a broad-band MCT detector and a KBr beamsplitter. Signal-averaged spectra of 250 or 2500 scans at 4 cm^{-1} resolution were recorded via attenuated total reflection techniques using one or two attachments. (The smaller number of scans corresponds to experiments on standards; the larger number corresponds to experiments on liquid chromatographic fractions.) Determination of extinction coefficients were performed using a variable angle 4$\times$ beam condensing attachment; examination of LC fractions was accomplished with a horizontal IRS attachment (both supplied by Harrick Scientific). In both cases, a germanium IRE was employed.

The liquid chromatography was accomplished using two systems. The bulk of the work was done on a Waters Associates high-pressure LC system equipped with two i0del 6000 pumps, a 660 solvent programmer, a 440 ultraviolet (UV) absorbance detector, and a UK6 injector. Additional chromatograms were collected and quantified using a Spectra Physics system composed of a SP8700 solvent delivery system, a SP4200 computing integrator, and an SP8440 XR variable-wavelength UV detector interfaced to an IBM XT computer. Separations were obtained using a linear water/THF gradient, and a reversed phase μ-Bondapak C-18 column supplied by Waters Associates. The solvent began at 20% THF to 80% water and was programmed to alter the solvent composition by increasing the percentage THF at a rate of 0.5% min^{-1}. The system flow rate was 2.0 ml/min, and detection was at 280 nm.

UV spectra were recorded on a Perkin Elmer Lambda 5 UV/VIS spectrophotometer interfaced to a Perkin Elmer 3600 data station. During the determination of molar extinction coefficients, 10-mm pathlength cells were used.

Results and Discussion

It is known that reversed phase liquid chromatography will separate chemical species based upon differences in the hydrophobic parts of the molecule.[11] This separation depends upon the relative solubility and distribution of the solute between the mobile and bonded phases. In addition to this chemical effect, in a reversed phase experiment the oligomers will

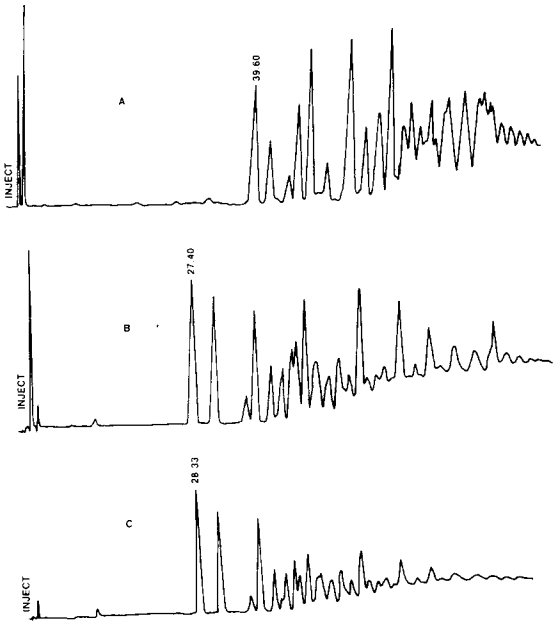

Fig. 1. Liquid chromatograms of resin systems A, B, and C.

also be separated based upon oligomeric molecular weight.[11,12] Generally, as the oligomeric molecular weight increases, the retention time of the eluting species increases.[12] The chromatograms of extracts from systems A, B, and C are shown in Figure 1. Each peak in C is duplicated in B; however, differences in peak intensities are apparent. The chromatogram of the extract of system A is dramatically different in that the apparent distribution is clearly shifted toward higher oligomeric molecular weights.

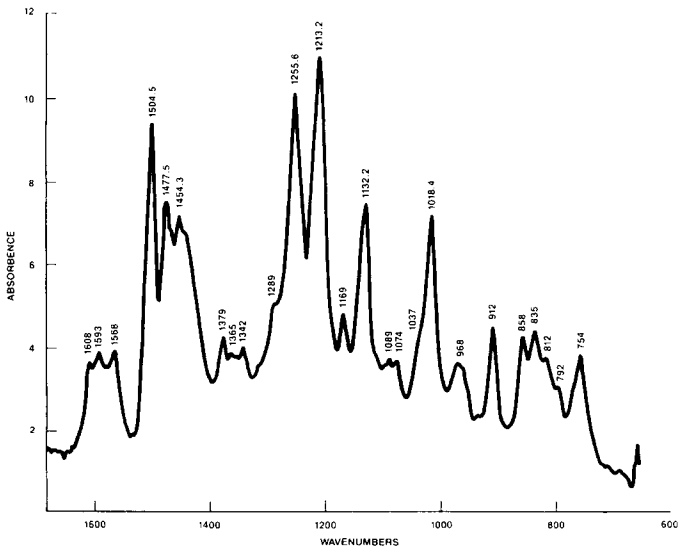

Fig. 2. The infrared spectra of an LC fraction of sample C eluting at 66.3 min.

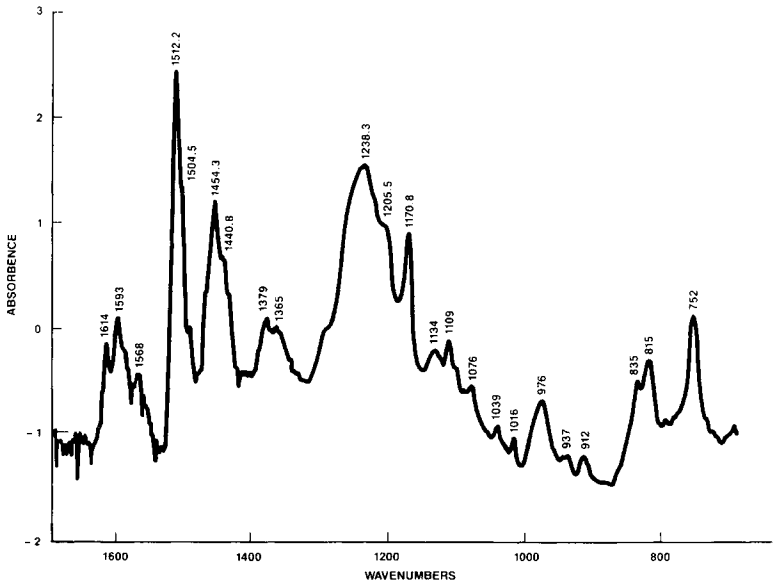

Fig. 3. The infrared spectra of an LC fraction of sample eluting at 42.1 min.

It was of interest in these systems to define the molecular weight distribution (MWD) of both the ECN and PFN resins present. Prior to specifying these distributions, it was necessary to first examine the chemical makeup of those peaks defining the chromatograms.

The infrared spectra for each of the collected fractions of samples A, B, and C collected had one of two general appearances. Examples of these two types of spectra are given in Figures 2 and 3. Figure 2 is the spectrum of a fraction of sample C eluting late in the chromatogram (retention time =

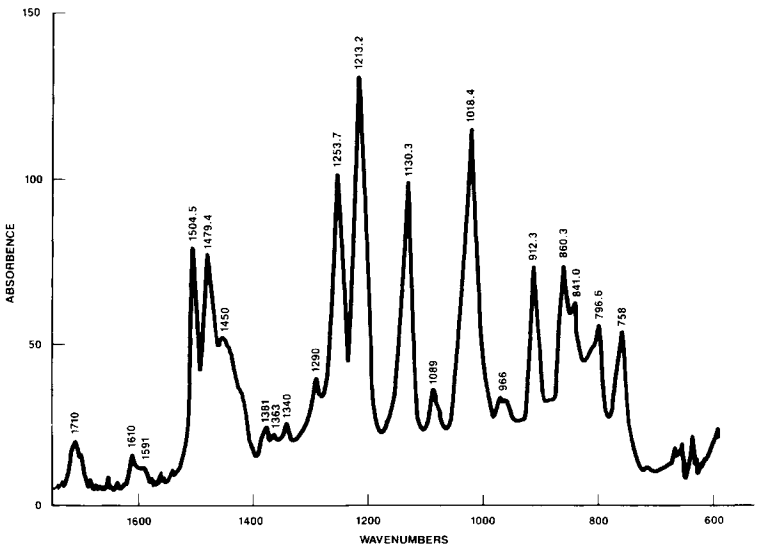

Fig. 4. The infrared spectra of Ciba-Geigy ECN1273.

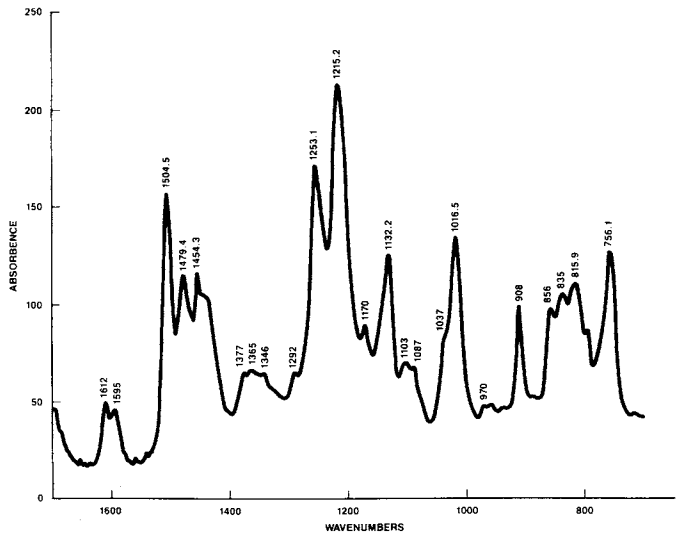

Fig. 5. The infrared spectra of Schenectady chemicals PFN resin HRJ1166.

66.3 min); Figure 3 represents a peak eluting early (retention time = 42.1 min). The spectrum of the ECN standard is given in Figure 4. There is a close resemblance to the spectrum of Figure 2. The spectrum of the PFN standard is given in Figure 5, and its resemblance to the spectrum of Figure 3 should be noted. There are peaks in Figures 2 and 3 that do not appear in the spectra of the corresponding matching standard, in particular the absorbance at 1169 cm^{-1} in Figure 2 and the peaks at 1130 and 976 cm^{-1} in Figure 3. The reason for this discrepancy is that each of the LC fractions consists of a mixture of ECN and PFN components. This can be verified by

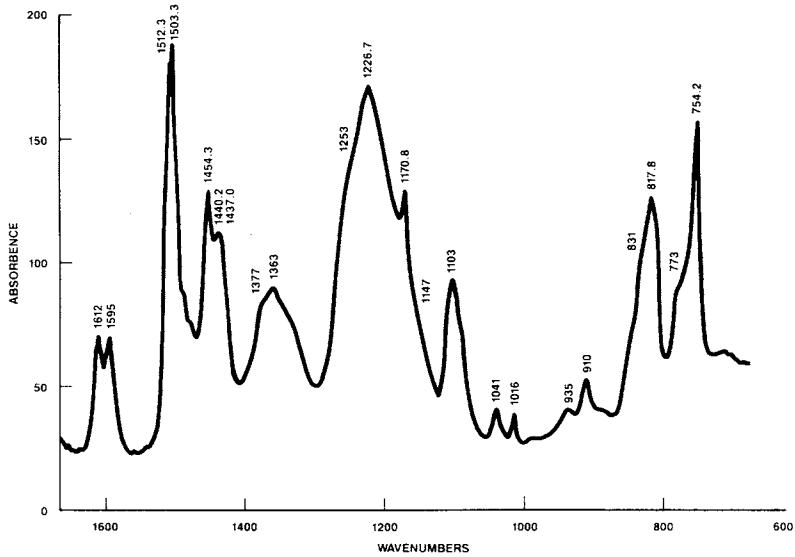

Fig. 6. Summation spectra of ECN 1273 + PFN HRJ1166. Weighting factor for the PFN component is 0.5 times that for the ECN component.

examining the summation spectrum in Figure 6. In this spectrum the standards are summed, with the PFN component receiving 0.5 times the weight of the ECN standard. The complete duplication of the spectrum in Figure 2 can now be observed. A similar reconstruction of the spectrum in Figure 3 occurs upon manipulation of the weighting factor. It is interesting to note that the chromatography does not separate the ECN and PFN components based upon differences in the substituents attached to the backbone aromatic ring, but rather is based upon differences in the oligomeric molecular weight. This complicates a description of the MWD of these components in molding compound formulations.

Infrared Peak Assignments

During the chemical characterization of molding compounds, it is of interest to make peak assignments based upon (1) an examination of the materials prior to curing, (2) an examination of the materials both during and following cure, and (3) a comparison with suitable standards. This has been accomplished for resin systems A, B, and C over the spectral range from 4000 to 700 cm^{-1}.[9,10,13] It is important to note that the major peaks given spectral assignments are identical in each of the resin systems studied.

Figure 7 is a schematic representation of the structural changes effected in both the ECN and PFN resin components during cure in the presence of a tertiary amine. It can be seen that the major spectral features expected before cure can be listed as

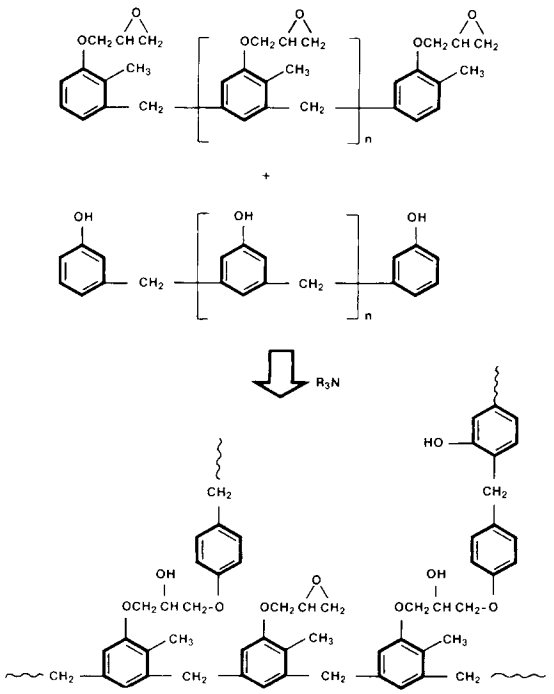

Fig. 7. Schematic representation of the reaction between an epoxy cresol novolac and a phenol formaldehyde novolac in the presence of a tertiary amine.

1). Trisubstituted aromatic with glycidal group (end group of ECN)
2). Tetrasubstituted aromatic with glycidal group (internal groups of ECN)
3). Disubstituted phenolic (PFN end group)
4). Trisubstituted phenolic (internal PFN groups)
5). Aryl-alkyl ether linkages
6). Epoxide group
7). Phenyl group
8). Phenolic hydroxyl (both free and H-bonded)
9). Ether methylene
10). Epoxide methylene
11). Epoxide -CH-
12). Cresylic methyl
13). Novolac methylene
14). Tertiary amine

Following cure we can expect a number of spectral alterations. These include
1). Increased aryl-alkyl ether
2). Increased alkyl hydroxyl (glycidal hydroxyl)
3). Decreasing or shifting phenolic hydroxyl (2 and 3-substituted)
4). Decreasing epoxide
5). Decreasing H-bonded hydroxyls
6). Decreasing amine bands due to catalyst complexation

In Table I, spectral alterations effected by system curing are listed in terms of an intensity increase or decrease. These changes are identical for each of the resin systems A, B, and C. Peak assignments are given in Table II. A convenient means for discussing these assignments is based upon the funcionality responsible for the absorbance, as well as upon the spectral region where the absorbance occurs.

In all unreacted materials a broad absorbance centered about 3350 cm^{-1} was assigned to H-bonded hydroxyls. This band shifted to approximately 3575 cm^{-1} and decreased significantly in intensity following cure. This shift is indicative of a decrease in the free hydroxyl associated with the PFN hardener before cure, and an increase in the restricted mobility alkyl hydroxyls associated with the glycidal group following cure.

The region 3100–2800 cm^{-1} contains the well-known CH stretching modes υ. The epoxide methylene υ (3005 cm^{-1}) decreases as expected following cure, but that for the ether methylene increases (2925 cm^{-1}). A new peak at 3025 cm^{-1} appears following cure and is attributed to the cured epoxy (CH-OH) C-H υ. A peak at 3057 cm^{-1} becomes resolved following cure and is assigned to the aromatic CH stretching vibration. The assymmetric and symmetrical methyl CH υ vibrations are assigned at 2956 and 2878 cm^{-1} respectively; the out-of-phase methylene CH υ is assigned at 2842 cm^{-1}. Other expected absorbances, such as $=C\text{-}O\text{-}CH_2$, CH_2 υ (in phase), are obscured by the strength of the above bands.

The four peaks at 1611, 1595, 1504, and 1456 cm^{-1} are assigned to the characteristic combined stretching and deformation aromatic C=C bands.

The spectral region between 1500 and 1300 cm^{-1} contains absorbances

TABLE I
Intensity Changes Following the curing of Epoxy Molding Compounds

Uncured peak (cm^{-1})	Cured peak (cm^{-1})	Intensity change
—	3025	Increase
3005	—	Decrease
2925	—	Increase
1595	—	Decrease
1504	—	Increase
1438	—	Decrease
1360	—	Decrease
1341	—	Decrease
1256	—	Decrease
—	1240	Increase
1230	—	Decrease
1210	—	Increase
1170	—	Decrease
1130	—	Increase
1103	—	Increase
1086	—	Decrease
1067	—	Decrease
1049	—	Decrease
—	1041	Increase
911	—	Decrease
833	—	Decrease

related to the deformation δ modes of the alkyl C-H band. Higher frequency bands are present for the aromatic CH δ peaks. The characteristic symmetrical and asymmetric methyl CH δ attributed to the cresol novolac C-CH_3 species are assigned at 1378 and 1475 cm^{-1}, respectively. The deformation vibrations of the epoxy –CH– and methylene groups are assigned at 1438 and 1341 cm^{-1}, and as can be seen in Table I these vibrations decrease in intensity following cure. The remaining CH δ modes are the novolac methylene (1456 cm^{-1}), the ether methylene (1323 cm^{-1}), the epoxide ether (1421 cm^{-1}), and the aromatic bands at 1289, 1017, 972, 888, 860, and 816 cm^{-1}.

The broad spectral range between 1400 and 800 cm^{-1} contains those vibrations arising within the carbon-oxygen and hydroxyl bonds. The aryl-alkyl ether (=C-O) C-O υ, and the aryl-alkyl ether (CH_2-O) C-O υ vibrations are assigned at 1210 and 1130 cm^{-1}, respectively. These absorbances both increase in intensity, as expected, following cure. The aryl ether C-O υ is assigned at 1256 cm^{-1}. An increase in this band is obscured because of the overlap of the epoxide C-O-C (1256 cm^{-1}), which decreases following cure. The ether linkages resulting from the strained epoxy ring have absorbances assigned at 1256, 1086, 911, and 833 cm^{-1}. These bands decrease following cure. The presence of alcohols can give rise to both C-O υ as well as to OH δ in this region. The phenolic OH δ is assigned at 1360 cm^{-1} and is observed to decrease following cure. The peak appearing at 1240 cm^{-1} following cure is assigned to the alkyl hydroxyl species. The phenol C-O υ frequencies are assigned at 1230, 1170, and 1103 cm^{-1}. These assignments are based upon examination of the model compounds, as well as the intensity variations seen during curing. The peak at 1103 cm^{-1} is obscured during cure because

TABLE II
Peak Assignments for Resin Systems A, B, and C

Peak position (cm^{-1})	Assignment
3575	Free hydroxyl, OH ν
3350	H-bonded hydroxyl, OH ν
3057	Aromatic CH ν
3025	Cured epoxy CH-OH, CH ν
3005	Epoxide methylene, $-CH_2-$, CH ν
2956	Methyl CH ν_{asym}
2924	Ether methylene O-CH_2, CH ν (in phase)
2878	Methyl CH ν_{sym}
2842	Methylene CH ν (out of phase)
1611	Aromatic skeletal ring breathing ν (1600 cm^{-1} band)
1595	Aromatic skeletal ring breathing ν (2d of 1600 cm^{-1} degenerate pair)
1512	Phenyl C_6H_5
1504	Aromatic skeletal ring breathing ν (1525–1475 cm^{-1} band)
1475	Methyl C-CH_3, CH δ_{asym}
1456	Methylene CH_2 δ; Aromatic skeletal ring breathing ν (1450 cm^{-1} band)
1438	Epoxide $-CH-$, CH δ; epoxide C-O ν
1421	Epoxide ether CH-O, CH δ
1378	Methyl C-CH_3, CH δ_{sym}
1360	Phenol OH δ (in plane)
1341	Epoxide methylene, $-CH_2-$, CH δ
1323	Ether methylene CH δ
1289	Epoxy aromatic CH δ
1256	Epoxide C-O-C; aryl ether C-O ν
1240	Alkyl hydroxyl OH δ
1230	Phenol C-O ν
1210	Aryl-alkyl ether =C-O, C-O ν
1170	Phenol C-O ν
1130	Aryl-Alkyl ether, CH_2-O, C-O ν
1103	Phenol C-O ν; secondary alkyl alcohol C-O ν
1086	Epoxide C-O-C
1067	Tertiary amine C-N ν
1049	Possible amine band
1041	Secondary alkyl alcohol C-O ν
1017, 972	Epoxy aromatic CH δ (in plane)
911	Epoxide C-O-C
888,860,816	Out-of-plane aromatic CH δ
833	Epoxide C-O-C
757	$-CH_2-$ skeletal vibration

of the increasing alkyl alcohol C-O ν assigned at the same location. This secondary alkyl alcohol is also observed to exhibit an absorbance located at 1041 cm^{-1}.

The bands present at 1067 and 1049 cm^{-1} appear to be due to the presence of the tertiary amine catalyst. Observation of standards and curing behavior

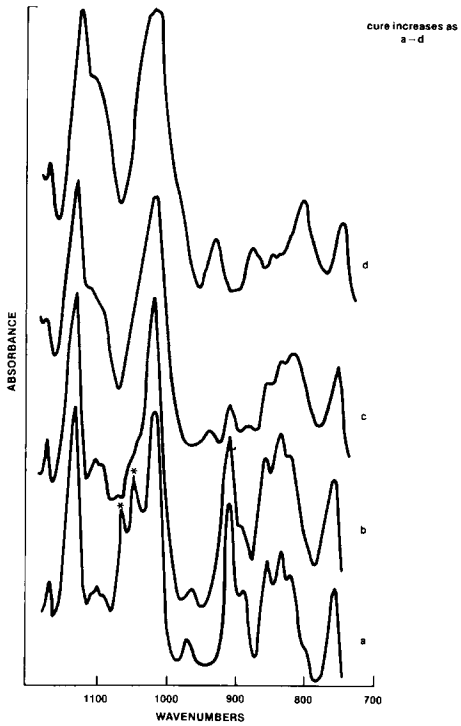

Fig. 8. Effect of cure on the 1100–1000 cm^{-1} region. The asterisk denotes the absorbance attributed to the tertiary amine.

support these assignments.[14,15] These bands were absent in the standards, and their behavior during cure is shown in Figure 8. The spectra in Figure 8 were recorded in a heated transmission IR cell. The peaks of interest decrease very easly in the reaction (Fig. 8b), followed by a broadening of the peak centered about 1018 cm^{-1}. This broadening is ascribed to the increase in the secondary akyl alcohol C-O υ.

Molecular Weight Distributions: ECN and PFN Resins

Molar Extinction Coefficients of the ECN and PFN Resins at 280 nm.

The detection of species eluting from the C-18 column was performed via UV absorbance measurements at 280 nm. Generally, as the oligomeric molecular weight of an eluting species increases, its retention time will increase.[12] Ideally, therefore, if the chromatographic separation were complete, the chromatogram would accurately describe the MWD. Since each of the peaks in the chromatograms represent a mixture of both ECN and PFN components, different molar extinction coefficients for these components will result in unequal contributions of each to the total UV absorbance of a given peak, A_{280}. This can be expressed by

$$A_{280} = l\,[\epsilon'_e\, X\, C_t + \epsilon'_p\, Y\, C_t] \tag{1}$$

where l = optical path length of the detector cell

ϵ'_e = molar extinction coefficient of the ECN resin at 280 nm
ϵ'_p = molar extinction coefficient of the PFN resin at 280 nm
X = percentage of ECN in the total concentration eluting
Y = percentage of PFN in the total concentration eluting
C_t = total concentration eluting for a given peak

As can easily be seen, the component percentages and molar extinction coefficients serve to determine the overall absorbance for a given peak. Since the component percentages vary from peak to peak, one must specify the contributions of the ECN and PFN oligomers to the total absorbance for each peak in order to specify the MWD.

Standards of the ECN and PFN resins were used to measure the molar extinction coefficients at 280 nm. The extinction coefficients are given by

$$\epsilon' = A_{280}/(1c) \tag{2}$$

where ϵ' is in units of $(\text{mol-cm/L})^{-1}$, and c is the standard solution concentration. A plot of A_{280} versus c will have a slope equal to $\epsilon' l$ if Beer's law is valid (i.e., if the plot is linear). Regression analysis of data collected between concentrations of 1×10^{-3} weight percent and 5×10^{-5} weight percent is given in Table III as a function of solvent composition. The correlation coefficients describe the linearity of each plot. The extinction coefficient as calculated from the slope after converting concentration in weight percent to moles/liter is given in Table IV as a function of solvent composition. It is evident from Table IV that the extinction coefficients are a function of solvent composition. In general, as the solvent power increases (i.e., percentage water decreases) the extinction coefficient increases for both the ECN and PFN resins. Our experiments utilize a linear gradient in solvent composition ranging between the extremes of 20:80 H_2O-THF and 80:20 H_2O-THF. Therefore, in order to calculate the correct contribution of a given peak to the total absorbance it is necessary to compensate for this varying extinction coefficient. The value of ϵ'_e does not change between 20 and 50% water. Thereafter, ϵ'_e decreases in a linear fashion according to

$$\epsilon'_e = -2.68(\%H_2O) + 237.16 \tag{3}$$

with $R = -0.984$. The value of ϵ'_p is unchanging between 20 and 40% water. Thereafter it decreases according to

$$\epsilon'_p = -4.10(\%H_2O) + 449.31 \tag{4}$$

with $R = -0.951$.

Percentage Contributions of ECN and PFN Oligomers to Chromatography Fractions.

The weight percents of ECN and PFN oligomers as described by the variables X and Y of eq. (1) were measured via FTIR spectroscopy coupled with the technique of attenuated total internal reflection. The infrared

TABLE III
Results of Linear Regression Analysis for A_{280} vs C as a Function of Solvent Composition

Resin	Solvent Composition		Slope	Intercept	R
	%H_2O	%THF			
ECN 1273	20	80	54.76	0.0032	0.9946
ECN 1273	40	60	59.59	0.0026	0.995
ECN 1273	50	50	54.78	0.0006	0.998
ECN 1273	60	40	47.39	0.0017	0.971
ECN 1273	70	30	29.23	−0.0007	0.996
ECN 1273	80	20	10.26	0.0008	0.988
HRJ 1166	20	80	244.25	0.0011	0.9985
HRJ 1166	40	60	259.87	0.002	0.999
HRJ 1166	50	50	228.58	0.0002	0.997
HRJ 1166	60	40	217.35	0.0016	0.999
HRJ 1166	70	30	124.92	0.0105	0.955
HRJ 1166	80	20	120.26	0.0020	0.996

absorbance of the ECN and PFN resins at a given wavelength, $A\lambda$ can be expressed as

$$A\lambda = \epsilon\lambda\, l\, c \tag{5}$$

where $\epsilon\lambda$ is the molar extinction coefficient of the ECN or PFN resin at a wavelength λ, l is the IR cell pathlength, and c is the concentration of absorbing species. In order to quantify the composition of a thin film deposited from a LC fraction solution upon an internal reflection element, it was necessary to measure ϵ for both the ECN and PFN resin standards. This was accomplished using a variable-angle 4× beam condensing attachment and germanium internal reflection elements (IRE). The interaction of an incoming and reflected IR beam experiencing total internal reflection is such that a standing wave, that is, continuous across the interface separating the sample and the IRE, is established. The depth of penetration

TABLE IV
Molar Extinction Coefficients for ECN and PFN Resins at 280 nm as a Function of Solvent Composition

Resin	Solvent Composition		Molar Extinction Coefficient (mol cm/1) × 10^{-4}
	%H_2O	%THF	
ECN 1273	20	80	0.9730
ECN 1273	40	60	1.0548
ECN 1273	50	50	0.9696
ECN 1273	60	40	0.8388
ECN 1273	70	30	0.5174
ECN 1273	80	20	0.1820
HRJ 1166	20	80	2.6135
HRJ 1166	40	60	2.7806
HRJ 1166	50	50	2.4460
HRJ 1166	60	40	2.3256
HRJ 1166	70	30	1.3367
HRJ 1166	80	20	1.2870

of this evanescent wave d_p, defined as the distance required for the electric field amplitude to fall to e^{-1} of its value at the surface, is given by

$$d_p = \frac{\lambda/n_1}{2\pi\,[\sin^2\theta - (n_2/n_1)^2]^{0.5}} \tag{6}$$

where n_1 and n_2 are the indices of refraction of the denser and rarer medium, respectively, and θ is the internal angle of incidence. One can therefore vary the depth of penetration of the sampling radiation by altering θ or by changing the ratio n_2/n_1. Altering d_p is analogous to changing concentration, thus ϵ can be determined from an experiment where θ is varied. The wavelengths of 1170 and 1130 cm^{-1} were chosen as representative of the PFN and ECN resins respectively (see Table II), and d_p was calculated considering the use of Ge IRE of differing entrance aperture angles. A correction was applied in those cases in which nonnormality of the incident IR beam to the entrance aperture results in reflection losses.

Equation (5) can be altered to re-express the absorbance by

$$A_\lambda = N d_p \epsilon \tag{7}$$

where N is given by

$$N = \frac{L}{t}\cot\theta \tag{8}$$

and represents the number of internal reflections in an IRE of length L and thickness t. In eq. (7) the product of the path length and concentration has been replaced by the number of internal reflections multiplied by d_p. We are not, therefore, calculating a molar extinction coefficient given in units of $(\text{mol-cm/L})^{-1}$. We are calculating a quantity with units of cm^{-1}. However, both effectively represent a concentration-dependent function (since the film thickness $\gg d_p$). The value measured in cm^{-1} can thus be used to calculate component percentages, since it will provide an equivalent weighting function. Using data collected with the ECN and PFN standards, we can calculate ϵ_e and ϵ_p from the slopes of absorbance versus d_p plots. These results are given in Table V. The percentage ECN and PFN can now be evaluated from

$$\%\text{ECN} = X = \frac{I_{1130}/e_e}{(I_{1130}/\epsilon_e) + (I_{1170}/\epsilon_p)} \tag{9}$$

$$\text{and PFN} = Y = 1 - X \tag{10}$$

ECN and PFN Resin MWD for Resin Systems A, B, and C.

The variables ϵ'_e, ϵ'_p, X, and Y, which allow us to calculate the contribution of a given LC peak to the total UV absorbance A_{280}, have been given. We can substitute for the measured absorbance of a given peak at 280 nm

TABLE V
Extinction Coefficient for the Epoxy Cresol Novalac (ECN 1273) and Phenol Formaldehyde Novalac (HRJ 1166) Resins

Resin	ϵ	Correlation coefficient
ECN 1273	2.41	0.999
HRJ 1166	0.78	0.841

a value normalized to the total UV absorbance A'_{280}. Equation (1) can now be rewritten to yield

$$C_t = \frac{A'_{280}}{l[(\epsilon'_e X/177) + (\epsilon'_p Y/107)]} \tag{11}$$

C_t is given in units of g/Liter instead of mol/Liter since we have divided the quantities $\epsilon'_e X$ and $\epsilon'_p Y$ by the appropriate conversion factors (i.e., 177 g/Eq of ECN and 107 g/Eq of PFN). Plotting $C_t/\Sigma C_t$ versus ΔRT will now yield the molecular weight distribution of the ECN and PFN combined. These values can be separated simply by plotting $XC_t/\Sigma C_t$ and $YC_t/\Sigma C_t$ as a function of ΔRT. ΔRT is the difference in retention times between a given peak and the first major peak to elute in these systems. Comparison of $XC_t/\Sigma C_t$ and $YC_t/\Sigma C_t$ versus ΔRT for the different samples therefore allows a direct comparison of the MWD.

The results for resin systems A, B, and C are given in Figures 9, 10, and 11. The overall distribution of oligomers as shown in Figure 9 demonstrates significant differences among the materials examined. In particular, resin C shows a rather even distribution of oligomeric molecular weights as one progresses from low MW (small ΔRT) toward higher MW (longer ΔRT). Resin B illustrates a decrease in the lower MW oligomers, with a concomitant increase in the moderately high MW oligomers with ΔRT between 30 and 40 min. Oligomers eluting at $\Delta RT > 45$ min are largely absent in this material. Resin A demonstrates a dramatic difference from the others.

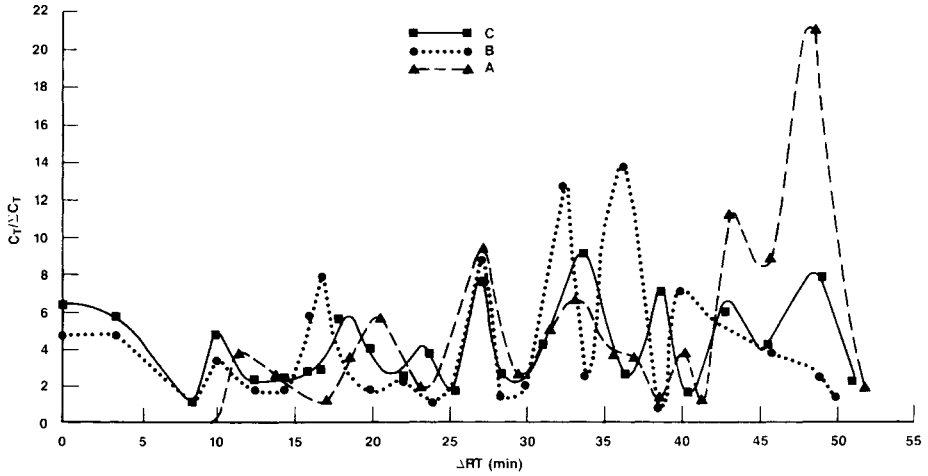

Fig. 9. MWD for the combined resin systems of the samples investigated.

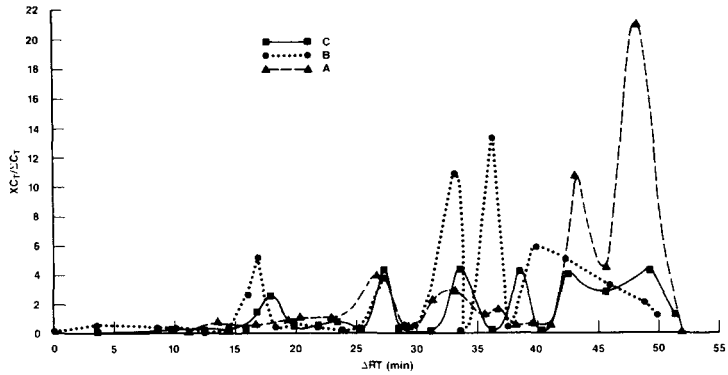

Fig. 10. MWD for the ECN components of the systems examined.

Material eluting with ΔRT < 10 min is completely absent, and the total distribution is shifted heavily toward the highest MW observed. An examination of the ECN and PFN component distributions further highlights differences in these materials. The epoxy components in resin system C are evenly distributed between ΔRT of 15 and 55 min. The bulk of the epoxy components in resin system B reside in the ΔRT range between 30 and 40 min. Once again resin system A has its emphasis at the highest MW values observed. The PFN resin components also show some interesting variations among these materials. Resin C places primary importance upon the lowest MW oligomers. Resin B also shows a distribution favoring lower MW oligomers, and for the most part ignores those oligomers with ΔRT > 35 min. The distribution measured in resin A is centered about 25 min with a complete absence of materials with ΔRT < 10 min.

One can, from the raw data used in the construction of the above plots, derive the stoichiometric ratios of ECN to PFN in the three systems of

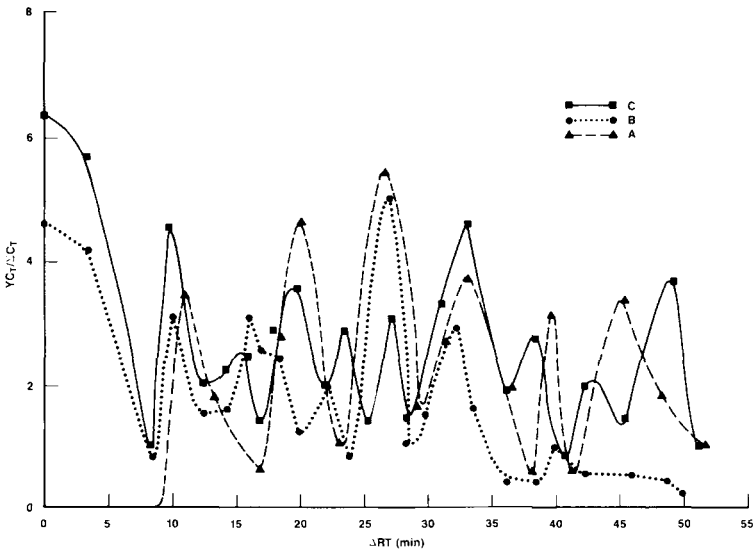

Fig. 11. MWD for the PFN components of the systems investigated.

interest. The contributuion of the epoxy to the stoichiometry will be $\Sigma(XC_t/\Sigma C_t)$, and that of the phenolic hardener is $\Sigma(YC_t/\Sigma C_t)$. The values so calculated are given in Table VI along with those values measured with the resin extracts via IR spectroscopy. The difference between resin system A and the others is noteworthy.

The results presented here demonstrate significant differences in both the resin and hardener molecular weight distributions, as well as the apparent resin-hardener stoichiometry. Let us briefly address these issues.

A distribution of molecular weights in the prepolymer should affect the cross-link density in the final network. In fact, a broadening of the transition region in cured epoxies has qualitatively been attributed to this effect.[16] Misra et al.[2] have examined the effects of cross-link density and cross-link density distribution upon a number of properties that determine the engineering behavior of high-T_g epoxies. In particular, a distribution in the molecular weights between cross-links M_c, was found to affect T_g, the slope of the transition region at T_g, the height and breadth of tan δ, and the characteristic creep time. The rubbery modulus, soluble content, ratio, density, and transition were all found to be influenced by the value of M_c, but not its distribution.

An interesting model was proposed by Misra et al.[2] to explain the morphological and mechanical differences observed in primary amine-cured DGEBA resins as a function of stoichiometry. Basically, small primary microgels are formed prior to the onset of gelation. These primary particles exhibit a distribution of sizes depending upon epoxy-hardener stoichiometry. After a certain concentration has been achieved, these primary particles agglomerate, via loose linkages, to form secondary microgels. The number of primary particles forming a secondary nucleus will determine both the size and coherence of the secondary particle. Thus, there will also be a distribution in the sizes of the secondary microgels that is intimately related to the original stoichiometry. At a critical concentration of secondary microgels, the experimental gel point is reached. At this point a phase inversion occurs, and the unreacted or partially reacted species become the dispersed phase within which further reaction occurs. It was proposed that the coherence of the final network depends strongly upon the linkages between the secondary microgels, a property that is strongly influenced by stoichiometry.

Hagnauer et al.[1] examined the effect of stoichiometry upon the curing behavior of a TGMDA-DDS epoxy system using gel permeation chroma-

TABLE VI
Stoichiometric Ratios of Epoxy to Phenolic Hardener for the Materials Examined[a]

Material	Epoxy-hardener stoichiometry	
	LC fractions (IR)	Starting material (IR)
Resin system A	1:1.44	—
Resin system B	1:1.30	1:1.55
Resin system C	1:3.06	1:2.84

[a] Values are defined in mol/L.

tography (GPC) and differential scanning calorimetry (DSC). They observed that increasing the epoxy-amine equivalent ratio decreased the rate of reaction, lowered the degree of conversion at the gel point, increased the extent of cross-linking, and led to higher final extents of reaction.

Keenan and Seferis[17] examined the effects of moisture and stoichiometry upon the dynamic mechanical properties of a DDS-cured TGDDM epoxy. The α transition was strongly influenced by the amount of DDS used. The low-temperature β transition was dependent upon moisture content, shifting to lower temperatures with increasing moisture. This shift was increased with increasing amounts of DDS. The ω transition was strongly dependent upon moisture content, and the mechanism assumed responsible for this transition supported the idea that moisture was preferentially absorbed in regions of low cross-link density. The cross-link density is of course intimately related to the stoichiometry.

Additional references can be found in the literature concerning the effects of stoichiometry[18,19], and prepolymer structure.[20,21] However, there is very little published on the system of interest in this study. Let it suffice to say that the molecular weight distributions of both the epoxy cresol novolac and the phenol formaldehyde novolac, as well as the stoichiometry of these components in the systems of interest, should play a major role in determining the properties of the cured system. It is the intent of future work within our laboratory to address the effect of the above-mentioned variables upon both high-pressure and ambient pressure reaction kinetics in filled ECN-PFN-tertiary amine systems. An understanding of system chemistry and reactivity will be complemented by the elucidation of structure-property relationships as determined via dynamic mechanical properties. One could from a study of this nature hope to approach our goal of linking material chemistry and properties with service behavior in these systems.

Conclusions

Infrared spectroscopy allows a complete chemical description of the resin systems studied; however, it does not offer a means of discriminating differences between systems in the fully cured state. Peak assignments are offered for the systems studied over the spectral range from 4000 to 700 cm^{-1}.

Each of the fractions separated during a reversed phase LC experiment, using the conditions cited in this paper, is a mixture of ECN and PFN resin components. This highly complicates an analysis of MWD.

The MWD can be determined in full utilizing a combination of techniques. These include liquid chromatography, Fourier transform infrared spectroscopy, and UV spectroscopy. An analysis of the type described herein will yield the weight percentage of the component of interest as a function of retention time, thereby completely describing the MWD. The overall distribution of molecular weights shifts toward oligomers of higher molecular weight as we progress in sequence from system C to A. Differences among the systems examined are also obvious if one examines the MWD of the ECN and PFN components, as well as the apparent ECN-PFN stoichiometry.

References

1. G. L. Hagnauer, P. J. Pearce, B. R. LaLiberte, and M. E. Roylance, Cure kinetics and mechanical properties of a resin matrix in *Chemorheology of Thermosetting Polymers*, C. A. May, Ed., ACS Symposium Series #227, ACS, Wasington, D.C., 1983, pp 25–49.

2. S. C. Misra, J. A. Manson, and L. H. Sperling, Effect of crosslink density distribution on the engineering behavior of epoxies and Network morphology and the mechanical behavior of epoxies, in *Epoxy Resin Chemistry*, R. S. Bauer, Ed., ACS Symposium Series #114, ACS, Washington, D.C., 1979, pp. 137–183.

3. S. L. Kim, J. A. Manson, and S. C. Misra, Creep behavior of amine cured epoxy networks: Effect of stoichiometry, in *Epoxy Resin Chemistry*, R. S. Bauer, Ed., ACS Symposium Series #114, ACS, Washington, D.C., 1979, pp. 183–197.

4. M. Ilavsky, L. M. Bogdanova, and K. Dusek, Formation, structure, and elasticity of loosely crosslinked epoxy-amine networks. II. Mechanical and optical properties, *J. Polym Sci., Polym. Phys. Ed.*, **22**, 265 (1984).

5. M. Shimbo, N. Nishitani, and T. Takahama, Mechanical properties of acid-cured epoxide resins with different network structures, *J. Appl. Polym. Sci.*, **29**, 1709 (1984).

6. A. M. Partansky, A study of accelerators for epoxy-amine condensation reaction, in *Epoxy Resins*, R. R. Gould, Ed., ACS Symposium Series #92, ACS, Washington, D.C., 1970.

7. E. Cuddihy and J. Moacanin, Dynamic mechanical properties of epoxies' β transition mechanism, in *Epoxy Resins*, R. F. Gould, Ed., ACS Symposium Series #92, ACS, Washington, D.C., 1970.

8. L. Buckley and D. Roylance, Kinetics of a sterically hindered amine-cured epoxy resin system, *Polym. Eng. Sci.*, **22**(3), 166, (1982).

9. G. C. Stevens, Cure kinetics of a low epoxide/hydroxyl group ratio bisphenol A epoxy resin-anhydride system by infrared absorption spectroscopy, *J. Appl. Polym. Sci.*, **26**, 4259 (1981).

10. G. C. Stevens, Cure kinetics of a high epoxide/hydroxyl group ratio bisphenol A epoxy resin-anhydride system by infrared absorption spectorscopy, *J. Appl. Polym. Sci.*, **26**, 4279 (1981).

11. L. R. Snyder and J. J. Kirkland, *Introduction to Modern Liquid Chromatography*, Chap. 7, John Wiley and Sons, New York, 1979.

12. G. L. Hagnauer, Quality assurance of epoxy resin prepegs using liquid chromatography, *Polym. Composites*, **1**(2), 81, (1980).

13. L. J. Bellamy, *The Infrared Spectra of Complex Molecules*, Vol. 1, 3rd Ed., Chapham and Hall, London, 1975.

14. F. Ricciardi, W. A. Romanchick, and M. M. Joullie, Mechanism of imadizole catalysis in the curing of epoxy resins, *J. Polym. Sci., Polym. Chem. Ed.*, **21**, 1475 (1983).

15. L. Matejka, J. Lovy, S. Pokorny, K. Bouchal, and K. Dusek, Curing epoxy resins with anhydrides. Model reactions and reaction mechanism, *J. Polym. Sci., Polym. Chem. Ed.*, **21**, 2873, (1983).

16. L. E. Nielsen, Crosslinking-effect on physical properties of polymers, *J. Macromol. Sci.*, **C3**, 69 (1969).

17. J. D. Keenan and J. C. Seferis, Effects of moisture and stoichiometry on the dynamic mechanical properties of a high performance structural epoxy, *J. Appl. Polym. Sci.*, **24**, 2375 (1979).

18. T. Murayama and J. P. Bell, Relation between network structure and dynamic mechanical properties of a typical amine-cured epoxy polymer, *J. Polym. Sci., A-2*, **8**, 437 (1970).

19. T. Hirai and D. E. Kline, Effects of heat treatment on dynamic mechanical properties of nonstoichiometric, amine cured epoxy resins, *J. Appl. Polym. Sci.*, **17**(1), 31 (1973).

20. N. Hata and J. Kumanotani, Viscoelastic properties of epoxy resins. I. Effect of prepolymer structure on viscoelastic properties, *J. Appl. Polym. Sci.*, **15**(10), 2371, (1971).

21. R. E. Johnson and A. L. Fricke, Effects of anhydride structure on the chemical and physical properties of resins, Proc. Conf. Reinf. Plast./Compos. Div., Soc. Plast. Ind., 27,19F, 1 (972).

Received June 20, 1985
Accepted August 20, 1985